# Spatial variations in the frequency-magnitude distribution of earthquakes in the southwestern Okinawa Trough

Jing-Yi Lin[1,4], Jean-Claude Sibuet[1], Chao-Shing Lee[2], Shu-Kun Hsu[3], and Frauke Klingelhoefer[1]

[1]*Ifremer, Centre de Brest, B.P. 70, 29280 Plouzané, France*
[2]*Institute of Applied Geophysics, National Taiwan Ocean University, 2 Pei-Ning Road, Keelung 202, Taiwan*
[3]*Institute of Geophysics, National Central University, Chung-Li 32001, Taiwan*
[4]*Collège de France, Chaire de Géodynamique, Europôle de l'Arbois, Bat. Le Trocadéro - Aile Sud, BP 80, 13545 Aix en Provence cedex 4, France*

The relations between the frequency of occurrence and the magnitude of earthquakes are established in the southern Okinawa Trough for 2823 relocated earthquakes recorded during a passive ocean bottom seismometer experiment. Three high *b*-values areas are identified: (1) for an area offshore of the Ilan Plain, south of the andesitic Kueishantao Island from a depth of 50 km to the surface, thereby confirming the subduction component of the island andesites; (2) for a body lying along the 123.3°E meridian at depths ranging from 0 to 50 km that may reflect the high temperature inflow rising up from a slab tear; (3) for a third cylindrical body about 15 km in diameter beneath the Cross Backarc Volcanic Trail, at depths ranging from 0 to 15 km. This anomaly might be related to the presence of a magma chamber at the base of the crust already evidenced by tomographic and geochemical results. The high *b*-values are generally linked to magmatic and geothermal activities, although most of the seismicity is linked to normal faulting processes in the southern Okinawa Trough.
**Key words:** *b*-Values, southern Okinawa Trough backarc basin, slab tear, magma chamber.

## 1. Introduction

Located east of Taiwan, the southern Okinawa Trough (OT) is a portion of a young continental backarc basin that is at the end of the rifting stage (Sibuet *et al.*, 1998) (Fig. 1(a)). Normal faulting is a common tensional process evidenced by seismic reflection data (Sibuet *et al.*, 1998) and focal mechanism analyses (Fournier *et al.*, 2001; Kao and Jian, 2001; Kubo and Fukuyama, 2003). In the southern OT, the volcanic front of the Ryukyu subduction zone is located within the backarc basin (Sibuet *et al.*, 1998; Wang *et al.*, 2000) (Fig. 1(a)). The most obvious cluster of seamounts, which consists of more than 70 volcanoes, is located in the vicinity of 24.8°N; 122.8°E and is named the "Cross-backarc volcanic trail" (CBVT) (Sibuet *et al.*, 1998; upper-left inset in Fig. 1(a)). Based on the relocated hypocenter locations (Engdahl *et al.*, 1998), magnetic anomaly distributions (Hsu *et al.*, 2001) and depths of the magnetic basement (Lin *et al.*, 2004a), a slab tear has been identified along the 123.3°E meridian (Fig. 1(a)). However, despite the microseismicity in the southern Okinawa Trough being very high, the surrounding land stations are too distant to record this stab tear. Consequently, with the objective of gaining a better understanding of the nature and role of tectonic features in this region, we conducted a passive seismic ocean bottom seismometer (OBS) experiment in November 2003.

Ishimoto and Ida (1939) and Gutenberg and Richter (1944) introduced the relation between the frequency of occurrence and the magnitude of earthquakes. The commonly used form is $\log_{10} N = a - b\,M$, where $N$ is the cumulative number of earthquakes with a magnitude equal or larger than $M$, and $a$ and $b$ are constants. The parameter '*b*' is the slope of the best fitting line between the observed number of earthquakes at a given magnitude and the magnitude (e.g. Fig. 2(d)). Since its first formulation, many studies of the frequency-magnitude distribution (FMD) as a function of time and space have been performed. For example, volcanic areas are commonly associated with high *b*-values (Warren and Latham, 1970), and underlying magma chambers are also characterized by anomalously high *b*-values (Wiemer and Wyss, 1997; Wiemer *et al.*, 1998; Murru *et al.*, 1999). The *b*-value has been shown to be inversely proportional to stress in laboratory (Scholz, 1968) and in mines experiments (Urbancic *et al.*, 1992). Stress and indirectly confining pressure are parameters which strongly control the type of faults and *b*-values.

For example, normal faulting events (tensional stress) have systematically the highest *b*-values and thrust events (compressional stress) have systematically the lowest (Frohlich and Davis, 1993; Wiemer and Wyss, 1997; Schorlemmer *et al.*, 2005). The presence of melt and normal faults that induce the distribution of high *b*-values are both present in the southern OT (e.g. Sibuet *et al.*, 1998; Shinjo, 2003a, b). We have calculated the spatial distribution of *b*-values in order to gain an understanding of how these may account for this complex tectonic regime and compare these results with a $Vp/Vs$ ratio and *P*- and *S*-velocity tomographic inversion performed with the same earthquakes (Lin *et al.*, 2006a, accepted).
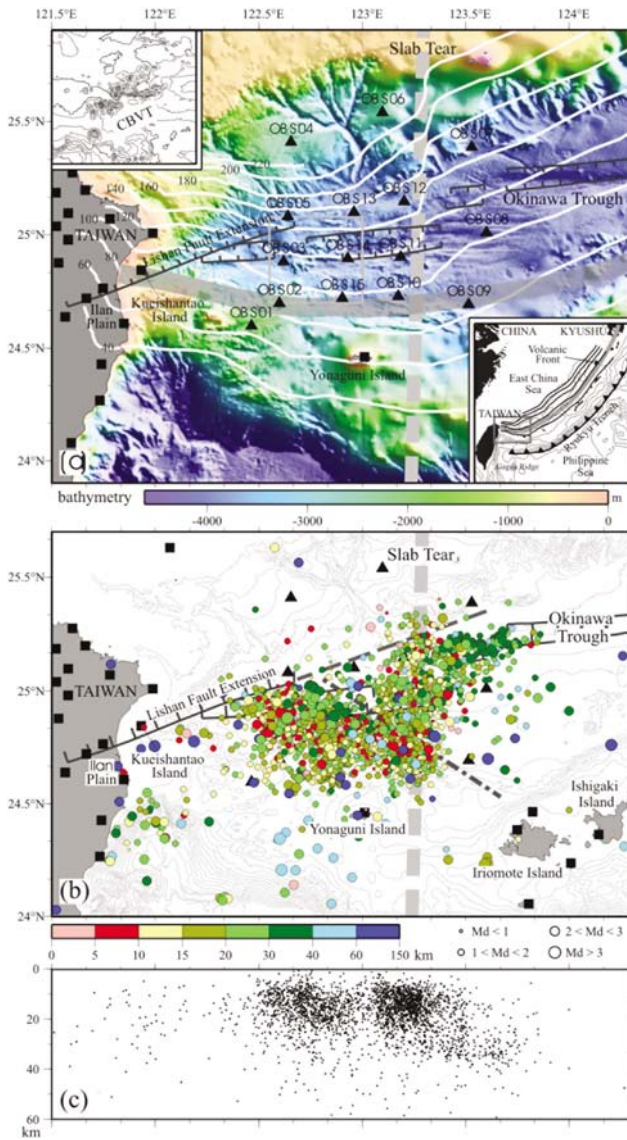
Fig. 1. (a) Map showing the simplified tectonic framework of the southern Okinawa Trough (OT). The locations of the Ryukyu trench and Okinawa Trough normal faults are from Sibuet and Hsu (2004). Upper-left corner inset: detailed bathymetric map (isobathic spacing, 100 m) of the cross-backarc volcanic trail (CBVT) (Sibuet *et al.*, 1998) located in the southern OT. The white contour lines are depths of the Wadati-Benioff zone (adapted from Font *et al.* (1999)). (b) Hypocenters of 2823 microearthquakes relocated with the *SIMUL2000* program in the southwestern OT during the 12-days acquisition period (Lin *et al.*, 2006b, revised). The size of dots is function of the magnitude. Colors show the depth ranges, with bathymetric contours every 100 m. The dashed line is the prolongation of the Lishan fault. Black triangles correspond to the locations of OBS stations, and black squares to surrounding land stations. The gray-colored dashed line shows the location of the slab tear. The large gray-colored line shows the location of the volcanic front. (c) E-W vertical cross section of the hypocenter distribution.

## 2. Data and Method

Fifteen OBSs were deployed in the southern OT from November 19 to December 1, 2003. More than 3300 microearthquakes were recorded during this 12-days passive seismic experiment (Fig. 1(b); Lin *et al.*, 2006b, revised). All *P*- and *S*- arrival times were picked by hand. As the amplitudes of the seismograms recorded by the OBS instruments were not calibrated, the magnitudes of the earth-

quakes were evaluated using the duration of seismic waves (Md) of other measurements (e.g. $M_L$, Md, Ms and Mw). The duration of each event was determined manually. The magnitudes of most of the earthquakes (Md) range from 1 to 2, although the whole range consists of magnitudes from 0.9 to 4 (Fig. 1(b)). This range in magnitude, dominated by small-magnitude earthquakes, provides an appropriate dataset to calculate *b*-values because the use of small-magnitude earthquakes increases the precision of *b*-values estimation (Wiemer and Wyss, 2002). In order to obtain accurately locate the hypocenters, all of the earthquakes were relocated using the *SIMUL2000* program (Thurber and Eberhart-Phillips, 1999). The layered model from the best VELEST solution was used (Kissling *et al.*, 1994) as the starting one-dimensional (1-D) model, and a minimal grid spacing of 15 km is used for the *SIMUL2000* program. Following the tomographic inversion, a detailed 3-D velocity model was obtained (Lin *et al.*, 2006a, accepted), and all of the earthquakes were relocated using this 3-D velocity model. Only hypocenters determined at an accuracy lower than 10 km in the three directions were chosen for the FMD calculations. In total, 2823 earthquakes were relocated. After relocation, the average rms residual decreases from 0.242 to 0.151 s, showing a better determination of hypocenters. Wiemer and Wyss (2002) have demonstrated that using earthquakes of different magnitudes (e.g. $M_L$, Md, Ms and Mw) may induce systematic errors. To avoid this problem, we only used the Md magnitude determined from the OBS stations, even if the available magnitude of the same earthquakes was calculated separately from the Taiwanese and Japanese networks.

Several areas with a $Vp/Vs$ higher than 1.78 are can be determined based on the tomographic results (Lin *et al.*, 2006a, accepted). Since the presence of melt or $H_2O$-enriched material is characterized by low $Vp$, low $Vs$ and high $Vp/Vs$ (Watanabe, 1993; Reyner *et al.*, 2006), we have highlighted such areas on Fig. 2(b) in white dashed contours. These high $Vp/Vs$ anomalies rise obliquely from a depth of 50 km through the slab tear in three directions (Fig. 3): a first branch rises northwesterly and feeds the CBVT; a second branch rises in a northerly direction above the slab tear to a depth of 15 km; a third branch rises to the north of Irimote Island (24.5°N; 123.9°E). The resolution estimates for the tomographic inversion are relatively high (>0.6) in the central part of the southern OT at a shallow depth (5-km). For the deeper part, the resolution decreases, but it is still acceptable beneath the Ryukyu Arc (>0.5).

*Zmap* software (Wiemer, 2001; Wiemer and Wyss, 1994, 1997) is used to estimate *b*-values at the nodal points of a 2-D grid using the 50 nearest earthquakes. The shape of the sampling volume is a vertical cylinder, and the grid spacing is 0.05°. The height of each sampling cylinder is 5 km, and the center of the cylinder corresponds to the depth of each estimated layer. The high-density hypocenter distribution allows us to use a grid spacing as small as 5 km in order to increase the spatial resolution. The resolution map corresponds to the radii of each circle of sampling (Fig. 2(c)): the larger the radius, the lower the chance of analyzing small sub-volumes. The magnitude of completeness (*Mc*) is a factor used to calculate the *b*- and *a*-values, which should
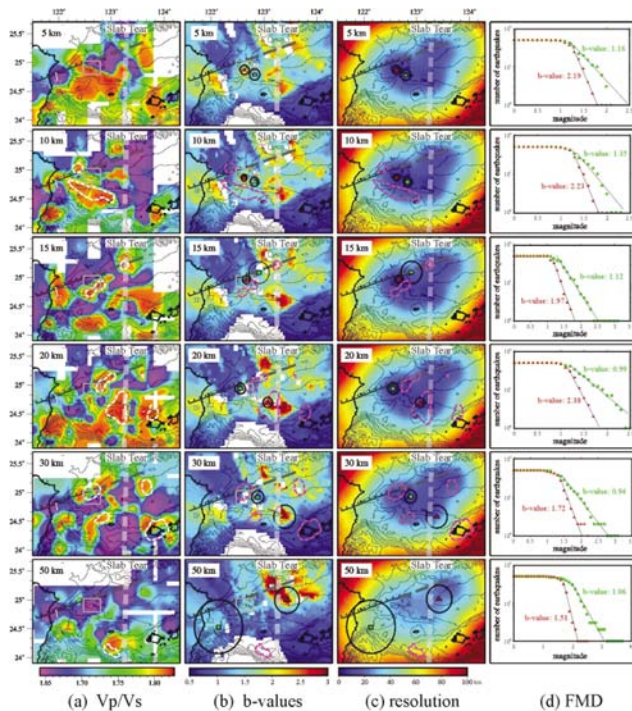
Fig. 2. (a) $Vp/Vs$ distribution in the southern OT displayed for six slices from 5 to 50 km. White dashed contours show areas where high $Vp/Vs$ and low $Vp$, $Vs$ velocities are observed on the tomographic results (Lin *et al.*, 2006a, accepted). The black dashed line shows the prolongation of Lishan fault. The light-colored dashed line shows the position of the slab tear. The light-gray square indicates the cross-backarc volcanic trail (CBVT). KI: Kueishantao Island. IP: Ilan Plain; (b) *b*-values distribution. The two circles with a red triangle and a green square in their centers define the volumes for which the frequency-magnitude relations are shown in (d). (c) Distribution of spatial resolution. Red, dashed contours shows the areas where high $Vp/Vs$ and low $Vp$, $Vs$ velocities are observed. (d) Comparison of frequency magnitude distribution (FMD) for the two circles located in (b) and (c). Black, straight lines show the best fitting lines whose slope is the *b* value.



Fig. 3. Geophysical distribution of areas with $Vp/Vs$ values higher than 1.78 and low $Vp$ and low $Vs$ values, extracted from slices of Figs. 6–8 and ranging from 10 km (light gray) to 50 km (dark gray) (Lin *et al.*, 2006a, accepted). Dashed lines are the isobaths of the Wadati-Benioff zone (adapted from Font *et al.* (1999)). Light-colored arrows show the upward propagation trends. V are the locations of detected hot vents (Lee, 2005). The black square indicates the cross-backarc volcanic trail (CBVT).

correspond to the maximum value of the FMD derivative for each sample. Instead of assuming a unique $Mc$ value, $Mc$ is automatically calculated according to the FMD in each sample. The suited $Mc$ value used for each sample under investigation allows us to correct *b*- and *a*- values estimations. The *b*-values estimations are finally obtained by using both maximum likelihood (Aki, 1965; Bender, 1983) and the weighted least squares methods. In this case, the results are independent of the method (Bender, 1983).

## 3. Results and Discussion

The 3-D mapping of *b*-values in the southern OT shows that within the crust the background *b*-value is approximately 1.1, with three embedded volumes characterized by $b>2.0$ (Fig. 2(b)). One of these major anomalies is located offshore the Ilan Plain, south of Kueishantao Island, at depths ranging from 0 to 50 km. The feeding process of the volcanic Kueishantao Island with melt and/or $H_2O$-enriched material rising from the Ryukyu slab edge has already been established from a previous tomographic study using earthquakes recorded by the Taiwanese network (Lin *et al.*, 2004b). We suggest that the high *b*-values correspond to the feeding channels imaged by tomographic results,
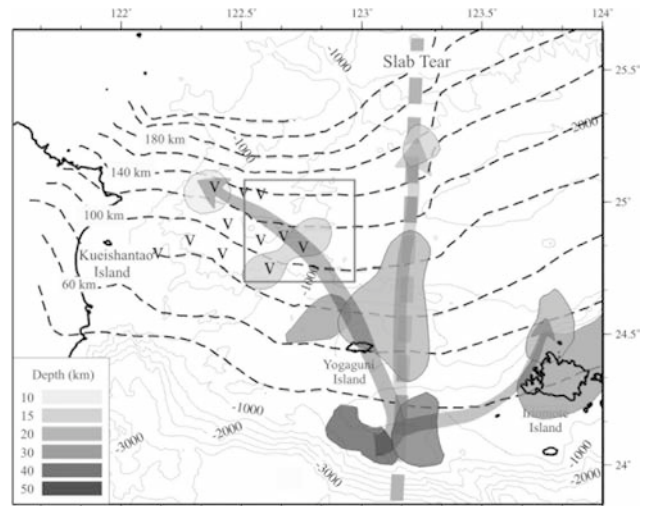
which rises up from a depth of 50 km to the surface in the direction of Kueishantao Island (Lin *et al.*, 2004b). However, the ∼40 km spatial resolution in this area (Fig. 2(c)) does not allow us to discuss this correspondence in more detail.

The most prominent anomaly in *b*-values corresponds to a volume of relatively high *b*-values located above the N-S trending slab tear in the vicinity of the 123.3°E meridian (Fig. 2(b)). This anomaly in high *b*-values ($>2.3$) is imaged at depths ranging from 0 to 50 km (Fig. 2(b)). At a depth of 50 km, part of this anomaly deviates eastward of the slab tear beneath the northern slope of OT. Glasby and Notsu (2003) reported the presence of a high heat potential along this N-S trending slab tear area. As mentioned previously, magmas and hot fluids in geothermal systems may induce high *b*-values (Wiemer and Wyss, 2002). We suggest that the high temperature of the inflowing mantle through the slab tear and the wedge may provide a high geothermal potential in this area. The anomalous heat originating from the slab tear may be transmitted to the overlying crust. In addition, such a heat transfer may also follow a magma conduit. This point will be discussed in the following section.

A vertical cylindrical body with high *b*-values, about 15 km in diameter, occurs at a shallow depth (0 15 km) beneath the CBVT (light-gray square, Fig. 2(a), (b)). The FMDs inside (red triangles) and outside (green squares) of this vertical cylinder show a large difference in *b*-values (∼2 and ∼1, respectively; see slices from 5 to 15 km in Fig. 2(d)), emphasizing the fact that *b*-values beneath volcanoes are generally smaller than previously thought and are distributed in pockets of anomalously high *b*-values embedded in a crust characterized by a mean *b*-value of ∼1 (e.g. Wiemer and Wyss, 2002; Power *et al.*, 1998; Murru *et al.*, 1999). According to the tomographic results, the low $Vp$, low $Vs$ and

and high $Vp/Vs$ anomalies at depths between 10 and 15 km suggest the existence of a magma chamber located beneath the CBVT area (Figs. 2(a) and 3) (Lin *et al.*, 2006a, accepted). Earthquakes are not generated within the magma chambers but around it. We thus interpreted the envelope of high *b*-values anomalies beneath the CBVT as the contours of the magma chambers. The mapped anomaly of *b*-values actually does include both the surrounding parts of magma chambers and the magma conduits to the surface (Fig. 3); however, it is located in the upper crust (0–10 km) and may also be linked to the presence of geothermal systems, as evidenced by tremor sources located in this area (Chang *et al.*, 2006, submitted) and by the distribution of hot vents in the southern OT (Lee, 2005; Chang *et al.*, 2006, submitted).

High $Vp/Vs$ and low $Vp$, $Vs$ anomalies have been identified in the southern OT (dashed contours in Fig. 2(a)–(c); Lin *et al.*, 2006a, accepted) and linked to the presence of melt and/or fluid-enriched material. At depths of less than 20 km, the distribution of the high *b*-values corresponds to the volumes surrounding the high $Vp/Vs$ and low $Vp$, $Vs$ anomalies. At larger depths ($>30$ km), the correlation between high *b*-values and high $Vp/Vs$ anomaly disappears. As mentioned in several former studies, stress is an important factor that affects the distribution of the *b*-values (Scholz, 1968; Wyss, 1973; Shaw, 1995) and may explain this discrepancy. Based on tomographic images, three sub-channels corresponding to melt and/or $H_2O$-enriched material rising from the slab tear have been identified (Lin *et al.*, 2006a, accepted). Two of the three conduits reach the upper crust of the southern OT (Fig. 3): one rises towards the northwest in the direction of the CVBT to a depth of 10 km where a magma chamber has been suggested from geochemical analyses of dredged rocks (Shinjo *et al.*, 2003a, b); the second rises to the north along the slab tear in the direction of the northern OT slope, to a depth of 15 km. The anomalies of high *b*-values mapped in our study at a shallow depth ($<30$ km) are in good agreement with the position of the two chambers. Hence, this comparison gives more credit to the fact that magmatic and/or geothermal activities might be the main factors controlling the distributions of high *b*-values. In addition, most of the anomalies of high *b*-values anomalies are not systematically located in the axial part of the southern OT, where numerous E-W trending normal faults account for the present-day extension in the OT (Sibuet *et al.*, 1998). High *b*-values underline features of volcanic or geothermal origin rather than the presence of numerous normal faults.

## 4. Conclusion

The distribution of small-magnitude earthquakes has been established from a passive seismic experiment in the southwestern OT. *b*-values were computed by using 2823 relocated earthquakes selected from this earthquakes dataset. Three volumes of high *b*-values were identified: (1) a first body characterized by $b\sim2$ is located offshore of the Ilan Plain, south of Kueishantao Island, and rises from the edge of the slab at a depth of 50 km to the surface, thereby confirming that the andesitic nature of rocks presents a subduction component (Chen *et al.*, 1995); (2) a second anomaly lies along the 123.3°E meridian, at depths

ranging from 0 to 50 km, above the Ryukyu slab tear, suggesting that high *b*-values are related to this feature; High temperature inflow passing through the slab tear might affect the overlying mantle and crust, and the heat anomaly might accelerate the generation of hot fluid in the geothermal system, resulting in high *b*-values; (3) a third body with a cylinder shape of about 15 km in diameter is identified beneath the CBVT, at depths ranging from 0 to 15 km; This anomaly is related to a magma chamber located at the base of the crust (10–15 km), as already suggested both by the tomographic results and the geochemical interpretation of dredged rocks. Though the seismicity in the southern OT is mainly controlled by normal faulting, high *b*-values are linked to volcanic and geothermal activities.

## References

Aki, K., Maximum likelihood estimate of b in the formula logN=a-bM and its confidence limits, *Bull. Earthq. Res. Inst., Tokyo Univ.*, **43**, 237–239, 1965.

Bender, B., Maximum likelihood estimation of *b*-values for magnitude grouped data, *Bull. Seismol. Soc. Am.*, **73**, 831–851, 1983.

Chang, T.-Y., J.-C. Sibuet, C.-S. Lee, and J.-Y. Lin, Tremors in the Southwestern Okinawa Trough., *Tectonophysics*, 2006 (submitted).

Chen, C. H., T. Lee, Y. N. Hsieh, C.-H. Chen, and W. Y. Hsu, Magmatism at the onset of back arc basin spreading in Okinawa Trough, *J. Volcanol. Geotherm. Res.*, **69**, 313–322, 1995.

Engdahl, E. R., R. D. Van der Hilst, and R. P. Buland, Global teleseismic earthquake relocation with improved travel times and procedures for depth determination, *Bull. Seismol. Soc. Am.*, **88**, 722–743, 1998.

Font, Y., S. Lallemand, and J. Angelier, Etude de la transition entre l'orogène actif de Taiwan et la subduction des Ryukyu—Apport de la sismicité, *Bull. Soc. Géol. Fr.*, **170**, 271–283, 1999.

Fournier, M., O. Fabbri, J. Angelier, and J.-P. Cadet, Regional seismicity and on-land deformation in the Ryukyu Arc: Implications for the kinematics of opening of the Okinawa Trough, *J. Geophys. Res.*, **106**, 13,751–13,768, 2001.

Frohlich, C. and S. Davis, Teleseismic b values: Or, much ado about 1.0, *J. Geophys. Res.*, **98**, 631–644, 1993.

Glasby, G. P. and K. Notsu, Submarine hydrothermal mineralization in the Okinawa Trough, SW Japan: an overview, *Ore. Geol. Rev.*, 23 (3-4), 299–339, 2003.

Gutenberg, R. and C. F. Richter, Frequency of earthquakes in California, *Bull. Seismol. Soc. Am.*, **34**, 185–188, 1944.

Hsu, S.-K., J.-C. Sibuet, and C.-T. Shyu, Magnetic inversion of the East China Sea and Okinawa Trough: Tectonic implications, *Tectonophysics*, **333**, 111–122, 2001.

Ishimoto, M. and K. Iida, Observations of earthquakes registered with the microseismograph constructed recently, *Bull. Earthq. Res. Inst.*, **17**, 443–478, 1939.

Kao, H. and P.-R. Jian, Seismogenic patterns in the Taiwan region: Insights from source parameter inversion of BATS data, *Tectonophysics*, **333**, 179–198, 2001.

Kissling, E., W. L. Ellsworth, D. Eberhart-Phillips, and U. Kradolfer. Initial reference models in local earthquake tomography, *J. Geophys. Res.*, **99**, 19635–19646, 1994.

Kubo, A. and E. Fukuyama, Stress field along the Okinawa Trough and the Ryukyu Arc inferred from moment tensors of shallow earthquakes, *Earth Planet. Sci. Lett.*, **210**, 305–316, 2003.

Lee, Y. L., The study of active submarine volcanoes and hydrothermal vents in the southernmost part of Okinawa Trough, Master thesis, National Taiwan Ocean University, Taiwan, 45 pp, 2005 (in Chinese).

Lin, J.-Y., S.-K. Hsu, and J.-C. Sibuet, Melting features along the Ryukyu slab tear, beneath the southwestern Okinawa Trough, *Geophys. Res. Lett.*, **31**, L19607, doi:10.1029/2004GL020862, 2004a.

Lin, J.-Y., S.-K. Hsu, and J.-C. Sibuet, Melting features along the western Ryukyu slab edge (northeast Taiwan): Tomographic evidence, *J. Geophys. Res.*, **109**, B12402, doi:10.1029/2004JB003260, 2004b.

Lin, J.-Y., J.-C. Sibuet, C. S. Lee, S.-K. Hsu, and F. Klingelhoefer, Origin of the southern Okinawa Trough volcanism from detailed seismic tomography, *J. Geophys. Res.*, 2006a (accepted).

Lin, J.-Y., J.-C. Sibuet, C. S. Lee, S.-K. Hsu, F. Klingelhoefer, Y. Auffret, P. Pelleau, and J. Crozon. Microseisismicity and faulting in the southwestern Okinawa Trough, *Tectonophysics*, 2006b (revised).

Murru, M., C. Montuori, M. Wyss, and E. Privitera, The location of magma chambers at Mt. Etna, Italy, mapped by b-values, *Geophys. Res. Lett.*, **26**, 2553–2556, 1999.

Power, J. A., M. Wyss, and J. L. Latchman, Spatial variations in frequency-magnitude distribution of earthquakes at Soufrière Hills volcano, Montserrat, West Indies, *Geophys. Res. Lett.*, **25**, 3653–3656, 1998.

Reyners, M., D. Eberhart-Phillips, G. Stuart, and Y. Nishimura, Imaging subduction from the trench to 300 km depth beneath the central North Island, New Zealand, with Vp and Vp/Vs, *Geophys. J. Int.*, 165(2), 565–583, 2006.

Scholz, C. H., The frequency-magnitude relation of microfracturing in rock and its relation to earthquakes, *Bull. Seismol. Soc. Am.*, **58**, 399–415, 1968.

Schorlemmer, D., S. Wiemer, and M. Wyss, Wariations in earthquake-size distribution across different stress regimes, *Nature*, **437**, doi:10.1038/nature04094, 2005.

Shaw, B. E., Frictional weakening and slip complexity in earthquake faults, *J. Geophys. Res.*, **100**, 18,239–18,252, 1995.

Shinjo, R., S. Hokakubo, S. Haraguchi, T. Matsumoto, and J. Woodhead, Geochemical characteristics of volcanic rocks from the southern Okinawa Trough and its implications for tectono-magmatic evolution, *EOS Trans. AGU*, **84**(46), Fall Meet. Suppl., Abstract V31E-0973, 2003a.

Shinjo, R., S. Hokakubo, S. Haraguchi, and T. Matsumoto, Regional variation in geochemistry of volcanic rocks from the southern Okinawa Trough, *Earth Mon.*, **43**, 21–26, 2003b (in Japanese).

Sibuet, J.-C., B. Deffontaines, S.-K. Hsu, N. Thareau, J.-P. Le Formal, and C.-S. Liu, The southwestern Okinawa Trough back-arc basin: Tectonics and volcanism., *J. Geophys. Res.*, **103**, 30,245–30,267, 1998.

Sibuet, J.-C. and S.-K. Hsu, How was Taiwan created?, *Tectonophysics*, **379**, 159–181, 2004.

Thurber, C. H. and D. Eberhart-Phillips, Local earthquake tomography with flexible gridding, *Comput. Geosci.*, **25**, 809–818, 1999.

Urbancic, T. I., C. I. Trifu, J. M. Long, and R. P. Toung, Space-time correlations of b-values with stress release, *PAGEOPH*, **139**, 449–462, 1992.

Wang, C., M.-L. Yang, C.-P. Chou, Y.-C. Chang, and C.-S. Lee, Westward extension of the Okinawa Trough and its western end in the northern Taiwan area: Bathymetric and seismological evidence, *Terr. Atm. Oc. Sci.*, **372**, 167–177, 2000.

Warren, N. W. and G. V. Latham, An experimental study of thermally induced microfracturing and its relation to volcanic seismicity, *J. Geophys. Res.*, **75**, 4455–4464, 1970.

Watanabe, T., Effects of water and melt on seismic velocities and their application to characterization of seismic reflectors, *Geophys. Res. Lett.*, **20**, 2933–2936, 1993.

Wessel, P. and W. M. F. Smith, Free software helps map and display data, *EOS Trans. Am. Geophys. Union*, **72**, 441–446, 1991.

Wiemer, S., A software package to analyze seismicity: ZMAP, *Seismol. Res. Lett.*, **72**, 373–382, 2001.

Wiemer, S. and M. Wyss, Seismic quiescence before the 1993 M=7.5 Landers and M=6.5 Big Bear (California) earthquakes, *Bull. Seismol. Soc. Am.*, **84**, 900–916, 1994.

Wiemer, S. and M. Wyss, Mapping the frequency-magnitude distribution in asperities: An improved technique to calculate recurrence times?, *J. Geophys. Res.*, **102**, 15,115–15,128, 1997.

Wiemer, S. and M. Wyss, Mapping spatial variability of the frequency-magnitude distribution of earthquakes, *Adv. Geophys.*, **45**, 259–302, 2002.

Wiemer, S., S. R. McNutt, and M. Wyss, Temporal and three-dimensional spatial analysis of the frequency-magnitude distribution near Long Valley caldera, California, *Geophys. J. Int.*, **134**, 409–421, 1998.

Wyss, M., Towards a physical understanding of the earthquake frequency distribution, *Geophys. J. R. Astr. Soc.*, **31**, 341–359, 1973.

J.-Y. Lin (e-mail: jylin@ifremer.fr, lin@cdf.u-3mrs.fr), J.-C. Sibuet, C.-S. Lee, S.-K. Hsu, and F. Klingelhoefer